



Lifetime prediction of plasma-sprayed thermal barrier coating systems

Shen Wei ^a, Wang Fu-chi ^{b,c}, Fan Qun-bo ^{b,c,*}, Ma Zhuang ^{b,c}

^a Central Iron and Steel Research Institute, Beijing 100081, PR China

^b School of Materials Science and Engineering, Beijing Institute of Technology, Beijing 100081, PR China

^c National Key Laboratory of Science and Technology on Materials under Shock and Impact, Beijing 100081, PR China

ARTICLE INFO

Article history:

Received 25 September 2012

Accepted in revised form 24 November 2012

Available online 4 December 2012

Keywords:

TBC

TGO

FEM

Lifetime prediction

ABSTRACT

Relying on the statistical treatment of the morphological characteristics of the interface between yttria stabilized zirconia (YSZ) top coat (TC) and metallic bond coat (BC), finite element model of thermal barrier coating (TBC) is generated by a sinusoidal function. Meanwhile, considering the thermally grown oxide (TGO) growth, creep effects and top coating sintering, lifetime prediction methodology is proposed. Furthermore, stress development during thermal cycling is calculated by finite element method (FEM). Comparing the numerically predicted TBC stresses with the failure stress of top coating, the lifetime of plasma-sprayed (PS) TBC is predicted between 810 and 900 cycles, in agreement with experimental result of about 860 cycles, the average data of 8 specimen lifetimes. Different factors to the failure of TBC are compared.

© 2012 Elsevier B.V. All rights reserved.

1. Introduction

Plasma-sprayed thermal barrier coatings have been widely applied to hot-section components in gas turbine to raise efficiency by increasing the maximum service temperature. However, during engine operation, several interrelated time and cycle dependent phenomena take place within the TBC failure by spallation of the top-coat [1]. Due to the effects of oxidation, creep and sintering on the local stresses responsible for the failure of TBC, it is hard to predict the lifetime of TBC.

Up to now, numerous studies for stress analysis and lifetime prediction of TBC systems have been reported [2–4]. These studies generally follow two main approaches, analytical approach and numerical approach. As to analytical approach [5–7], it is difficult to predict the stress development in the complex TBC system. Recently, a model based on micromechanical mechanisms to describe crack growth and failure of thermally cycled PS TBC was developed by Vassen and co-workers [8,9], however, the interactive effect of interface morphology, TGO growth, TBC creep, TC sintering and the thermal expansion mismatch cannot be considered. More concerns have been focused on numerical approach, especially on FEM [10–12]. Baker and co-workers [13–15] have proposed a parametric study of the stress state of TBC by considering creep relaxation and cooling stresses, the influence of the interface geometry on the stress is also studied by FEM. Busso and co-workers [16,17] have developed a software tool for lifetime prediction of TBC by FEM, which interpolates the finite element results with respect to time, temperature and a geometric parameter to predict key stresses that drive failure, and coating system lifetime. These works play

important role on TBC life prediction. However, the predicted local TBC stresses are somewhat large because some factors have not been considered.

In the present work, considering interface morphology, thermally grown oxide (TGO) growth, creep effects and top coating sintering, lifetime prediction methodology is proposed. Furthermore, stress development during thermal cycling is calculated by finite element method.

2. Thermal cycling experiments

The investigated TBC systems consist of zirconia partially stabilized with about 8 wt.% yttria (8YSZ) ceramic top coat and Ni–38.5Co–21Cr–8Al–0.5Y bond coat. With the basic operating parameters listed in Table 1, the nano-structured 8YSZ top coat [18] is produced by atmospheric plasma spraying (APS). The bond coat is deposited onto a disk shaped GH99 substrate by vacuum plasma spraying, and GH99 is a nickel-based DS (directional solidification) superalloy with nominal composition of Ni–17Cr–8.0Co–7.0W–2.4Al–1.0Ti. To minimize the effect of stresses originating at the free edge of the specimen, the disk shaped with a beveled edge is designed with about 35 mm diameter and 5 mm thickness.

Table 1
Basic operating parameters of plasma spraying.

	Primary gas (scf/h)	Second gas (scf/h)	Carrier gas (scf/h)	Electric current (A)	Spraying distance (mm)	Spraying thickness (mm)
Top coating	75	45	8	850	75	0.3
Bond coating	120	20	10	700	75	0.1

* Corresponding author at: School of Materials Science and Engineering, Beijing Institute of Technology, Beijing 100081, PR China. Tel.: +86 10 68911144.

E-mail address: fanqunbo@bit.edu.cn (F. Qun-bo).

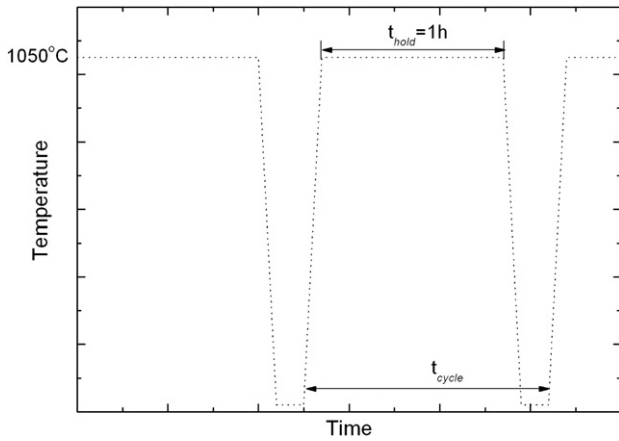


Fig. 1. Temperature history in thermal cycles.

Table 2
TGO thickness after different thermal cycles.

Thermal cycles	8	100	200	400	600	850
TGO thickness (μm)	1.62	3.25	4.14	5.21	5.65	6.50
Standard deviation	1.22	1.48	1.36	1.42	1.34	1.40

The specimens are subjected to thermal cycling using an infrared radiation furnace between the minimum cycle temperature T_{min} of 20 °C and the maximum cycle temperature T_{max} of 1050 °C. The thermal cycle has a heating rate of 3 °C/s, followed by a dwell period t_{hold} of 1 h at T_{max} , subsequent cooling to T_{min} with a rate of 3 °C/s and a final dwell time of 5 min at T_{min} , as illustrated in Fig. 1. Since the sample is with a relatively smaller size 35 mm \times 5 mm in the furnace, the temperature gradients in the specimen can be ignored.

2.1. TGO growth

The growth of the TGO is an important phenomenon responsible for the spallation failure of TBC. During isothermal oxidation in T_{max} , TGO forms and grows at the top coat/bond coat interface. A series of scanning electron microscopy (SEM) micrographs over 200 images at 2000 magnifications is taken to identify the TGO thicknesses for each statistical cycle number listed in Table 2. Fig. 2a–d shows typical SEM micrographs of TGO growth after different thermal cycles. For each SEM micrograph, the TGO thickness is measured by the TGO area over the curve length of TGO in micrograph. Subsequently, the statistical method is used to identify the average thickness of TGO. Quantitative data of TGO thickness is shown in Table 2, which shows that the average thickness of the TGO is 1.62 μm after 8 cycles. With thermal cycles and exposure time increasing, the TGO thickness increases. When thermal cycling increases to 850 cycles (850 hour exposure time), the average thickness of the TGO accumulation is up to 6.50 μm , which is approximately fourfold over the thickness after 8 cycles.

The following phenomenological relation was found to describe the general dependency of the TGO thickness h on the absolute maximum cycle temperature. While t_{hold} and n are dwell period and thermal cycles.

$$h = B \cdot (n \cdot t_{hold})^m \quad (1)$$

where B is a proportionality constant and m is a growth exponent. Fig. 3 shows TGO thickness on bond coat as a function of exposure isothermal time and temperature. Thus, in our research, the function can be quantified as

$$h = 0.86 \cdot n^{0.3} \quad (2)$$

here, h is TGO thickness, μm , n is thermal cycles, and $t_{hold} = 1$ h.

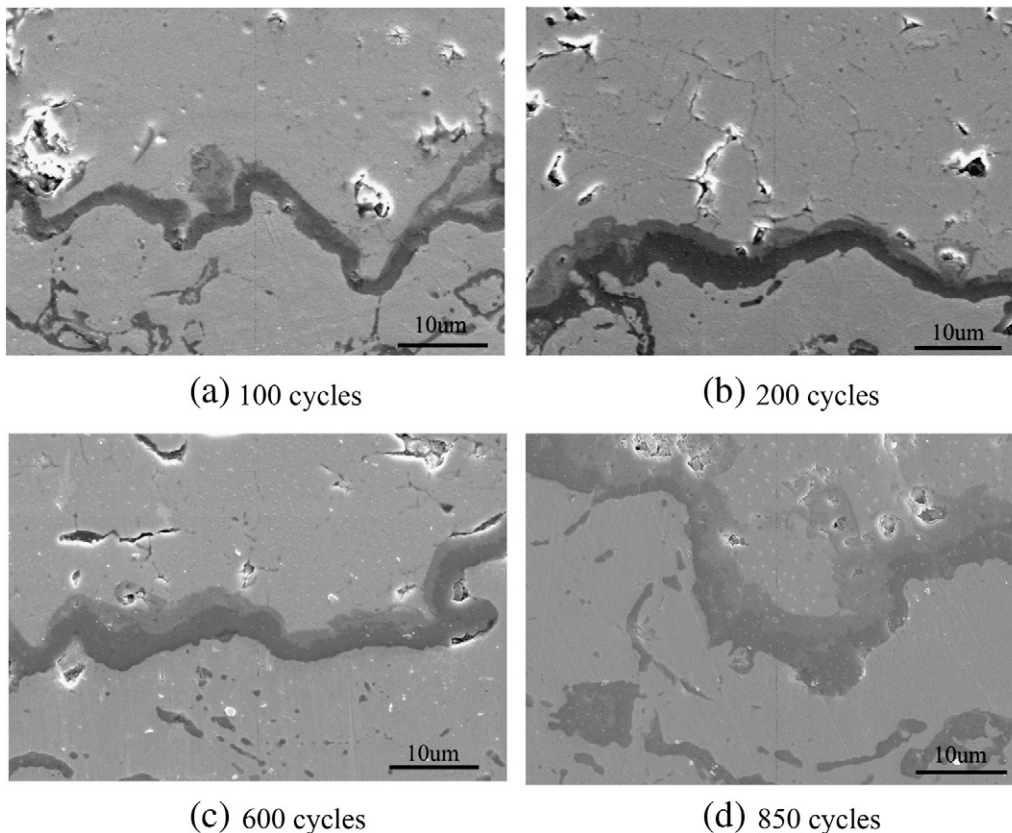


Fig. 2. Typical SEM micrographs of TBC after isothermal oxidation and thermal cycles revealing the growth of TGO. (a) 100 cycles; (b) 200 cycles; (c) 600 cycles; and (d) 850 cycles.

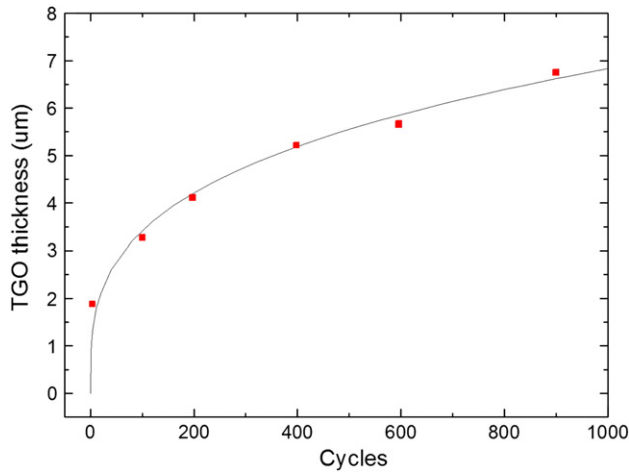


Fig. 3. TGO growth as a function of isothermal thermal time and temperature.

2.2. Failure modes and lifetime

When cracks can be observed in the surface of TBC by naked eyes, TBC is assumed to be a failure. Fig. 4 shows the delamination crack path from cross section after 860 thermal cycles, when failure occurs by spallation of the TC at or near TC/TGO interface. There are many reasons for TBC failure, mainly including [1] (1) roughening of the TC/TGO/BC interfaces, (2) TGO growth, (3) TBC creep, (4) TC sintering, (5) the thermal expansion mismatch between TC, TGO and BC, and so on. Considering of these reasons, FEM will be applied to model TBC stresses and predict lifetime in this work.

3. Lifetime prediction methodology

The finite element analysis is done with FEM code LS-DYNA. The three-dimensional cylindrical problem can be reduced to a two-dimensional mesh using general plain strain elements. The investigations presented here are confined to the peak of the maximum principal stresses of TBC, because we assume them to be responsible for crack initiation and crack propagation in early stage of TBC failure.

Fig. 5 shows the flow chart of TBC thermal cycling lifetime prediction program with FEM, which consists of 3 major steps.

- Step 1. Select series of SEM images from specimens, then obtain the cumulative probability of the morphological characteristics of the interface ($r(i)$), and subsequently determine the value of critical $r(i)$, followed by building finite element model with the TGO thickness changing between 0 and h , setting proper boundaries conditions.
- Step 2. Considering oxidation, creep and sintering, calculate the stress $\sigma_{(T_{max})}$ and strain $\varepsilon_{(T_{max})}$ of TBC during hold periods at T_{max} , select $\sigma_{(T_{max})}$ and $\varepsilon_{(T_{max})}$ when the TGO thickness is $(\Delta h \cdot i)$ as the initial stress and strain in the beginning of next cooling stage, then calculate the peak of stress during cooling, $\sigma_{(T_{min})}$.
- Step 3. If $\sigma_{(T_{min})} >$ failure stress, failure occurs, at the same time, the thickness of TGO is between $\Delta h \cdot (i-1)$ and $\Delta h \cdot i$, and the lifetime of TBC is between $\frac{1}{t_{hold}} \cdot \left(\frac{\Delta h \cdot (i-1)}{B}\right)^{\frac{1}{m}}$ and $\frac{1}{t_{hold}} \cdot \left(\frac{\Delta h \cdot i}{B}\right)^{\frac{1}{m}}$.

4. Finite element method to model TBC stresses

4.1. Finite element model and boundaries condition

During thermal cycling, the stress concentrating in the roughening interface is primarily responsible for TBC failure. As shown in Fig. 6,

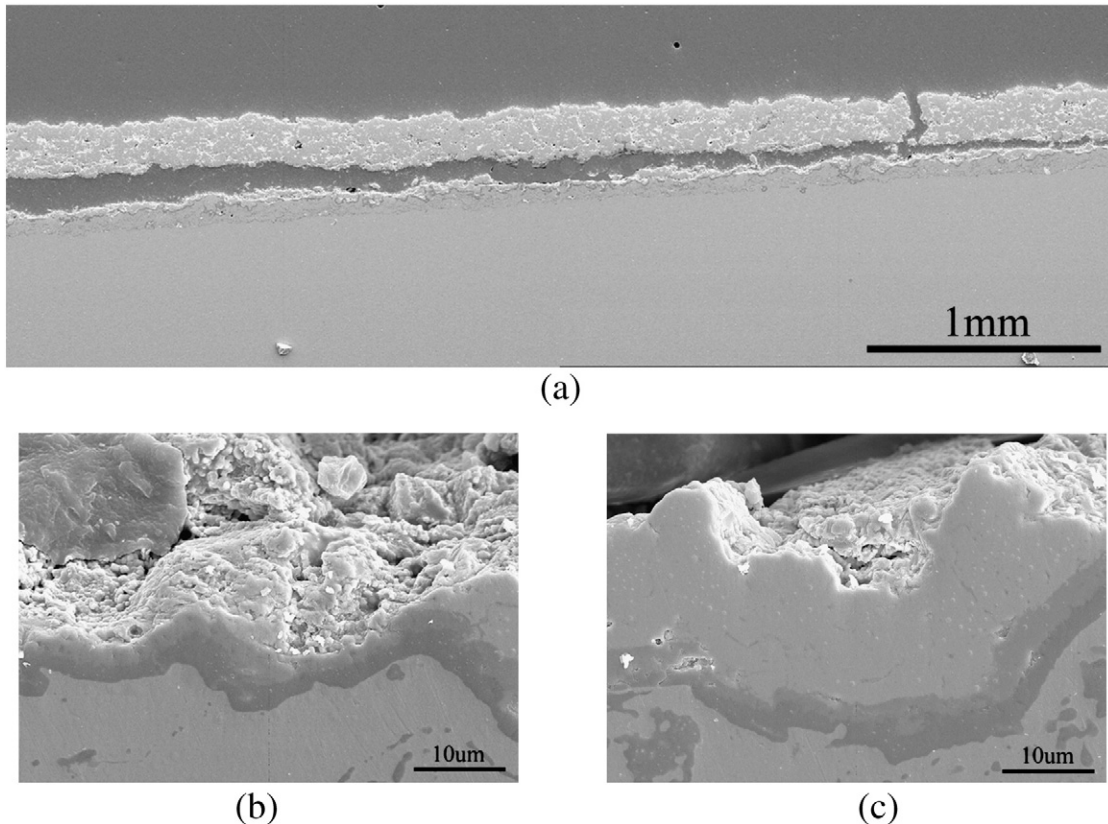


Fig. 4. SEM micrographs of TBC failure modes after 860 thermal cycles. (a) Failure mode at low magnification ($\times 50$) (b) failure at TC/BC interface ($\times 2000$) (c) failure near TC/BC interface ($\times 2000$).

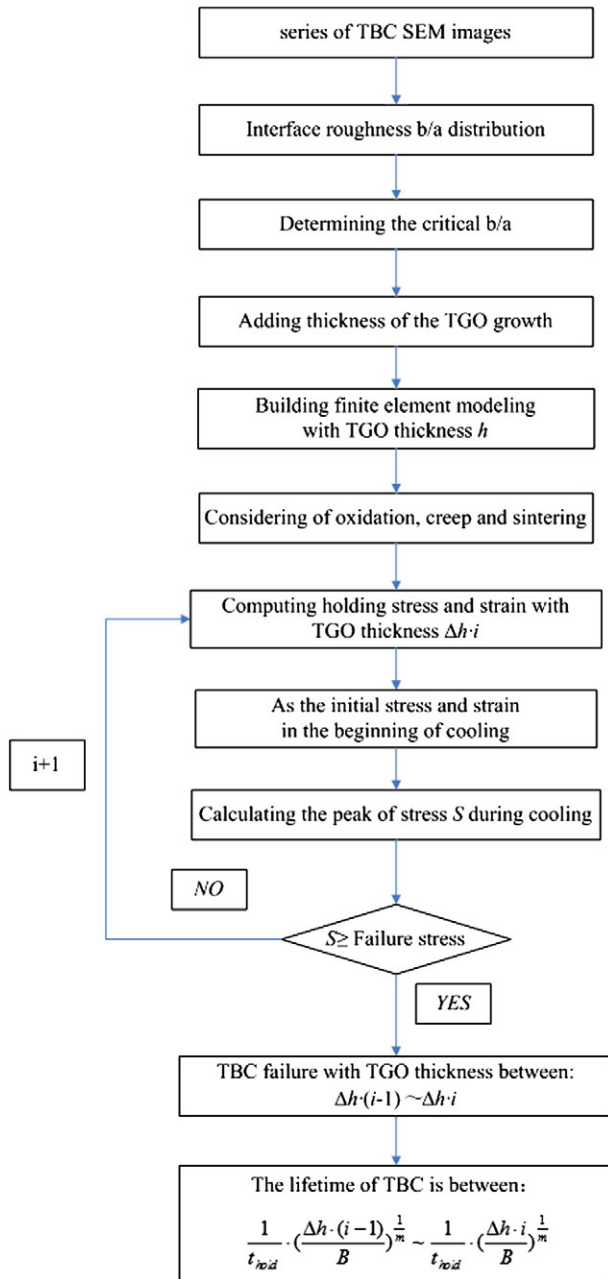


Fig. 5. The flow chart of TBC thermal cycling lifetime prediction program with FEM.

the morphological characteristics of the interface can be represented by the series of undulations. The random nature of the interface morphology can be ideally separated to number of unit cell, which is characterized by the half-period a and the amplitude b [13]. It should be noted that the b/a constitutes the most important roughness parameter [16]. The damage occurs where the value of b/a is largest, which means that larger b/a corresponds to more dangerous region in coating [17]. In order to obtain the cumulative probability of b/a , series of contiguous scanning electron microscopy (SEM) images taken along the cross-section are analyzed by the statistical quantitative method in conjunction with digital image processing. Fig. 7 illustrates the cumulative probability of the measured values $r(i)$, which represents different b/a , $r(i) = b(i)/a(i)$. In Fig. 7, symbols show part of the measurement data, and the smooth line is the cumulative normal distribution of the measured data. Busso and co-workers' research [17] shows that TBC failure can be taken as damage of more than 22%. Here, damage of 22% corresponds to critical value $b/a = 0.8$. Hence, finite element model with $b/a = 0.8$ is built to represent the whole coating during thermal cycling, see Fig. 8. Where the interface region is modeled with a sinusoidal geometry with the amplitude of $9.6 \mu\text{m}$ and half-period $12 \mu\text{m}$. The finite element mesh consists of 10,472 nodes and 10,280 quadrangle elements, and the meshing is very fine in the region of interface. 35 layers on the bond coat side of the interface have a thickness of only $0.2 \mu\text{m}$ each, and these elements will be changed from bond coat to TGO during the simulation to represent the TGO thickness growth from $0 \mu\text{m}$ to $7 \mu\text{m}$ during thermal cycling.

The nodes at $x=0$ are allowed to move in the x -direction, but the movement is coupled such that all these nodes have the same displacement, and do the nodes at $x=12 \mu\text{m}$. Thus the model can be considered as a slice taken out of a sample. Because of low heating and cooling rate, the temperature within TBC systems is assumed to be uniform. During 1 hour hold time at $1050 \text{ }^\circ\text{C}$ in the beginning of thermal cycle, all stresses relax quickly to near zero as a consequence of rapid creep in TC and BC, and the TBC system is considered to be stress free at $1050 \text{ }^\circ\text{C}$ in the beginning of simulation.

4.2. Material properties

Basic material data including Young's modulus E , Poisson's ratio ν , coefficient of thermal expansion (CTE) α , and yield stress σ_{yield} in the simulation are listed in Tables 3–5 [15,19,20]. As the simulation is isothermal at $1050 \text{ }^\circ\text{C}$, all nodes in the mode always have the same temperature, no thermal properties are needed at $1050 \text{ }^\circ\text{C}$.

With thermal cycles increasing, bond coat oxidation, TBC creep and TC sintering occur.

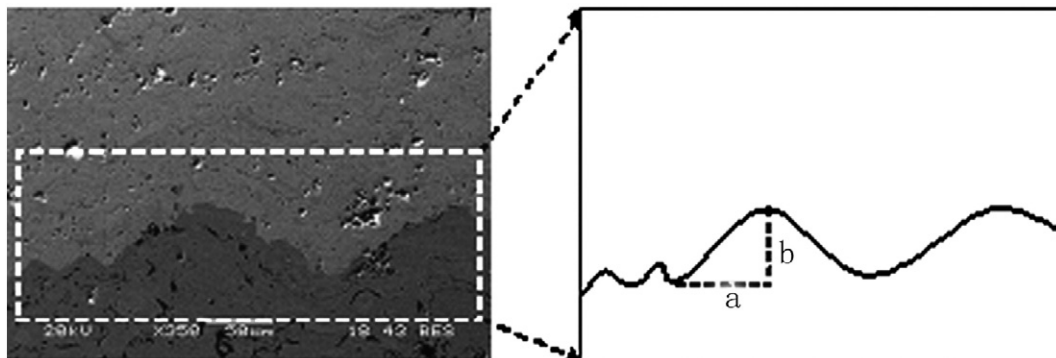


Fig. 6. Sketch illustration of geometric parameters a and b of the interface morphology characteristics.

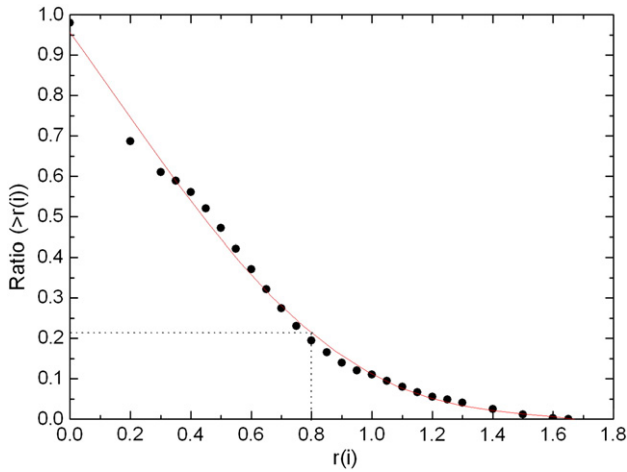


Fig. 7. Cumulative probability of $r(i)$.

(1) Bond coat oxidation

Due to the interconnected porosity existence in top coat and oxygen transparent property of the ZrO_2 -based top coat, bond coat oxidation and the formation of the TGO are inevitable. Throughout the paper, the TGO is assumed to consist of $\alpha-Al_2O_3$, for the oxidation of aluminum, and the reaction is as follows



The oxide formation is associated with isotropic swelling whereby the Pilling–Bedworth ratio $\varphi = 1.28$ of Al_2O_3 is taken. During isotropic swelling in simulation, the Al_2O_3 layer is compressed in y -direction of the specimen by 8.5%. The growth rate of TGO can be seen in 2.1.

(2) TBC creep

During hold time at 1050 °C, the creep rate of TC, BC and TGO are described by Eqs. (4)–(6) [19–21], respectively.

$$\dot{\epsilon} = 3.8E - 16 \cdot \sigma^{3.98} \quad (4)$$

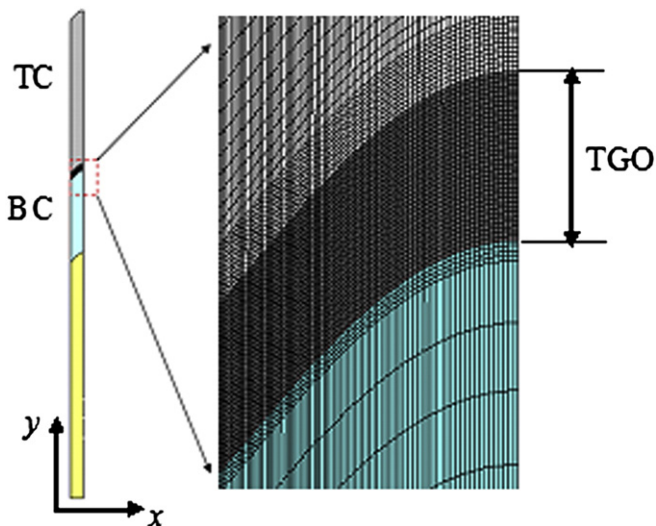


Fig. 8. The finite element model with $b/a=0.8$.

Table 3
Elastic properties of ceramic coating.

T (°C)	E (GPa)	ν	$\alpha (\times 10^{-6}/^{\circ}C)$
20	56	0.2	10.01
1100	25	0.2	10.02

Table 4
Properties of bond coating.

T (°C)	20	500	700	850	950	1050
E (GPa)	152	136	128	109	100	58
ν	0.311	0.334	0.342	0.347	0.350	0.352
$\alpha (\times 10^{-6}/^{\circ}C)$	12.3	15.1	15.9	17.0	18.0	19.4
σ_{yield} (MPa)	868	807	321	117	66	38

Table 5
TGO properties.

T (°C)	20	500	1000	1100
E (GPa)	400	375	325	320
ν	0.23	0.24	0.25	0.25
$\alpha (\times 10^{-6}/^{\circ}C)$	7.13	7.99	8.75	8.88
σ_{yield} (MPa)	8000	8000	300	300

$$\dot{\epsilon} = 1.5E - 7 \cdot \sigma^4 \quad (5)$$

$$\dot{\epsilon} = 7.3E - 4 \cdot \sigma^1. \quad (6)$$

(3) TC sintering

The increase of the Young's modulus E of TC due to sintering during hold time at 1050 °C can enhance the thermally induced stress and therefore strongly affects the performance of TBC system. The increase of E can be described by [8]

$$E(t) = \frac{\beta E^0 E^\infty}{\beta E^0 + E^\infty - E^0} \quad (7)$$

where,

$$\beta = 1 + A_{sint} \cdot \exp\left(-\frac{E_{sint}}{k_B T}\right) \cdot (n \cdot t_{hold})^n \quad (8)$$

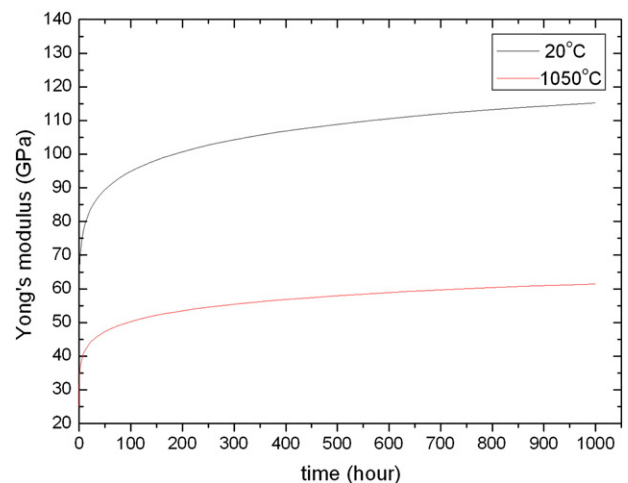


Fig. 9. The Young's modulus of TC with sintering time.

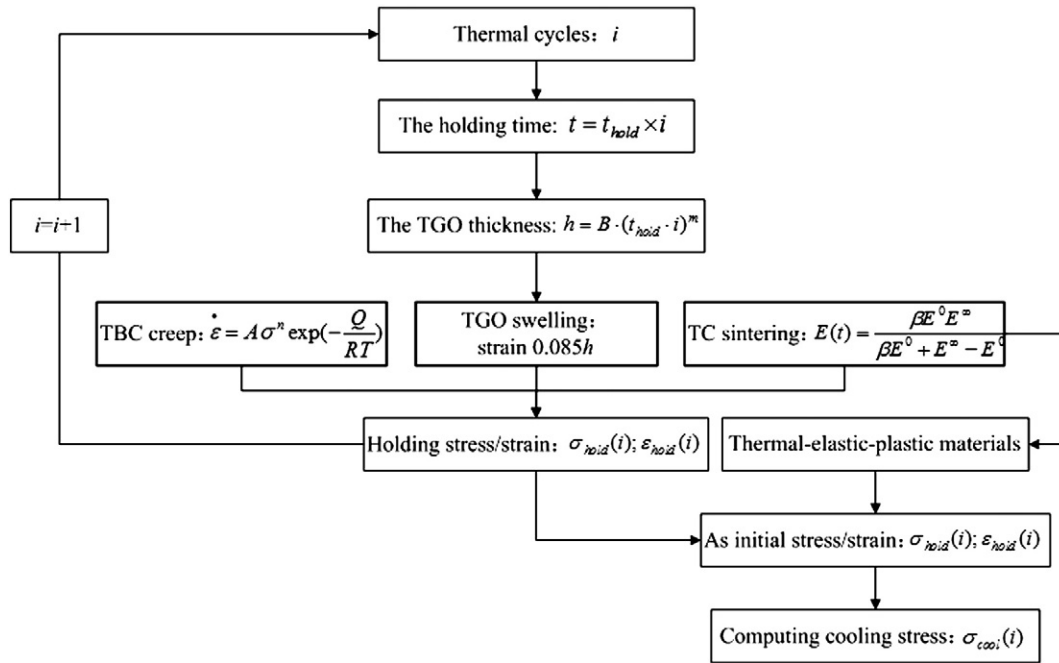


Fig. 10. The flow chart of TBC stresses simulation at *i* thermal cycles with FEM.

here, E^0 and E^∞ represent the starting and the bulk modulus, k_B is the Boltzmann constant, A_{sint} , E_{sint} and n are parameters to describe the sintering kinetics, $A_{sint} = 2 \times 10^{10}$, $E_{sint} = 3$ eV, $n = 0.25$ [8,20]. Fig. 9 shows the sintering time dependency of the Young's modulus of TC in our simulation.

4.3. Stress simulation in TBC

A generic thermal cycle includes three stages: heating from T_{min} to T_{max} , followed by a dwell period t_{hold} at T_{max} , subsequent cooling to T_{min} . Damage in the TBC mainly occurs during cooling due to thermal expansion mismatch stresses, so dwell periods and cooling stages are studied in this paper. Actually, the total stress during cooling consists of $\sigma_{creep-TGO} + \sigma_{sintering} + \sigma_{thermal}$. During dwell periods at T_{max} , the TGO growth results in a constrained volume expansion that leads to high stress, however, the creep can relax this stress efficiently, and the stress $\sigma_{creep-TGO}$ in TBC caused by oxidation and creep will persist at all temperature. During cooling stages, the stress $\sigma_{sintering}$ caused by the increased Young's modulus at 1050 °C due to sintering in TC will

be enhanced. Meanwhile, stress $\sigma_{thermal}$ caused by initial properties mismatch is considered to be unaffected by time. The flow chart of TBC stresses simulation at *i* thermal cycles with FEM is shown in Fig. 10. In LS-DYNA, the simulation is divided to two stages: firstly, calculating stress $\sigma_{hold}(i)$ and strain $\epsilon_{hold}(i)$ in hold time at 1050 °C with considering oxidation (TGO), sintering and creep. Then, keywords *INITIAL_STRESS and *INITIAL_STRAIN are applied to calculate $\sigma_{cool}(i)$ based on $\sigma_{hold}(i)$ and $\epsilon_{hold}(i)$. During thermal cycling, the TGO growth and the Young's modulus increasing are realized by full restart method.

As the experimental results show that spallation of TC results in the failure of TBC ultimately, only TC stress is discussed in this paper. The peaks of the maximum principal (1st) stresses σ_{peak} at room temperature after different thermal cycles are shown in Fig. 11. It is obvious that before 900 cycles (the TGO thickness in 0–6.6 μm), σ_{peak} increase rapidly, however, from 900 to 1100 cycles (the TGO thickness in 6.6–7.0 μm), the peaks of 1st stresses decline slightly. Different factors to the peaks of 1st stresses are computed and compared in Fig. 12. Without considering of oxidation (TGO), sintering and creep, $\sigma_{thermal}$ is constant with different thermal cycles.

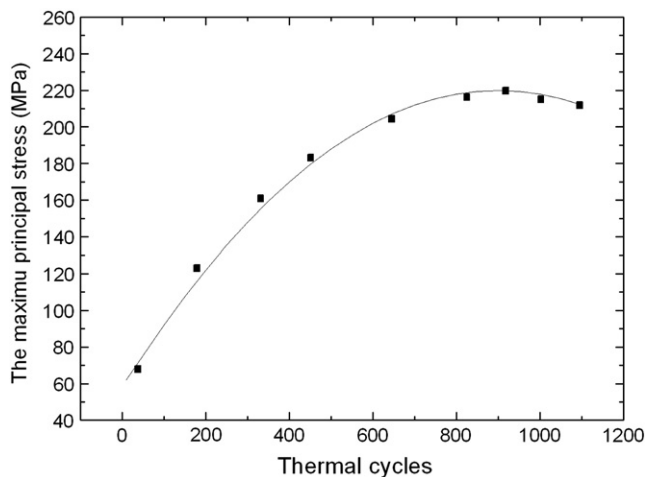


Fig. 11. The peaks of the maximum principal stresses after different thermal cycles.

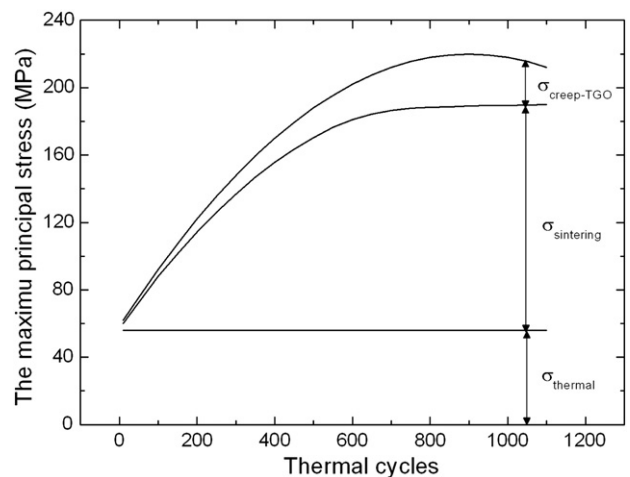


Fig. 12. Comparisons of different factors to peaks of the maximum principal stresses in TC.

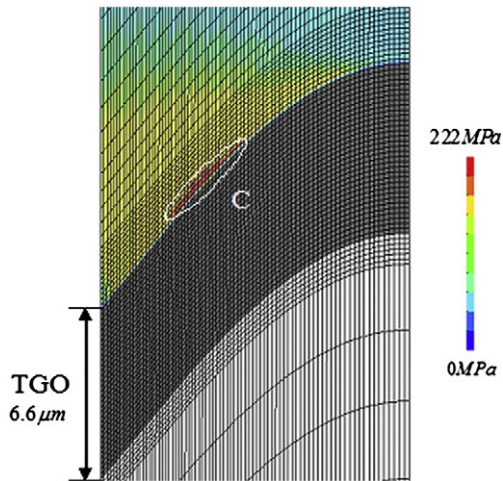


Fig. 13. The maximum principal stresses in TC with 900 thermal cycles.

Without considering of oxidation (TGO) and creep, $\sigma_{sintering}$ will always increase due to the increase of the Young's modulus. Before 900 cycles, because the oxidation rate is high compared to the rate of creep relaxation, $\sigma_{creep-TGO}$ increases during the hold periods, consequently, σ_{peak} in Fig. 11 increases during cooling. After 900 cycles, Fig. 9 indicates that the increment of the Young's modulus is nearly 0, so $\sigma_{sintering}$ keeps constant nearly. Meanwhile, creep relaxes the TC stress induced by oxidation due to the declining of oxidation rate, subsequently, $\sigma_{creep-TGO}$ declines, consequently, σ_{peak} decreases during cooling.

Fig. 13 shows the 1st stress distribution in TC at room temperature during 900 cycles. The peak of 1st stress reaches 222 MPa in region C, where is the most vulnerable part in TBC. According with the simulation results, microcrack growth observed in the similar region where is away from macrocracks observed in the surface of TBC by naked eyes is shown in Fig. 14 after 850 cycles.

4.4. Lifetime prediction

In our previous study [22], the fracture tensile stress of 8YSZ in TC is found to be 215 MPa. Comparing with Fig. 11, during 810–900 cycles, the peak of 1st stresses in TC will reach the failure stress, hence, the lifetime of TBC is determined between 810 and 900 cycles with the TGO thickness between 6.4 and 6.6 μm , which agrees with experimental average lifetime 860 cycles. In the present work, because the interface model with periodic boundary conditions is effectively modeled as infinite series of undulation morphological characteristics $r(i)$, the TBC life predicted by FEM can reflect the experimental result effectively. It should

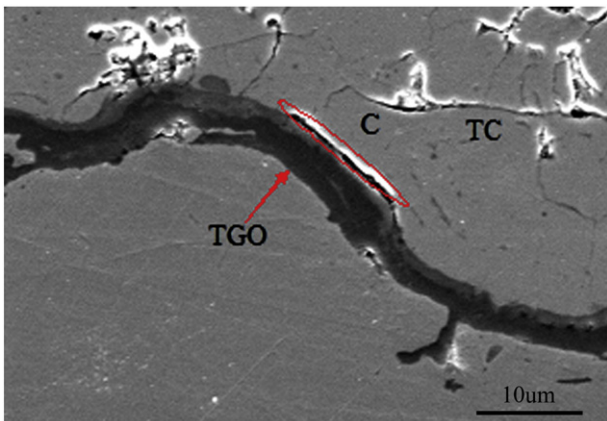


Fig. 14. Crack growth in similar region C.

be noted that total TBC life is expected by FEM to be higher than the cycle number at which localized microcracks at single locations occur, because the process of crack growth until complete failure which is hard to simulate is unconsidered in this study. Failure of TBC cannot be completely described by a simple model, it is a complex process. Other factors, such as uneven TGO thickness, process of microcracks growth, are also important to precisely character TBC failure mechanism.

5. Conclusions

- (1) According to experimental studies of the TBC lifetime during thermal cycling, the function of the TGO growth is quantified, what is more, failure occurs by spallation of the TC at or near TC/TGO interface, and the TBC average lifetime is found to be 860 cycles. The random nature of the interface morphology can be ideally separated to number of unit cell, which is characterized by the half-period a and the amplitude b . Based on statistical, finite element model with $b/a=0.8$ is built to represent the overall coating.
- (2) Considering oxidation, creep and sintering, lifetime prediction methodology is proposed with LS-DYNA code. It is obvious that before 900 cycles (the TGO thickness in 0–6.6 μm), the peaks of the maximum principal stresses increase rapidly, however, from 900 to 1100 cycles (the TGO thickness in 6.6–7.0 μm), the peaks of the maximum principal stresses decline slightly. Comparing to the failure stress in TC, the lifetime by FEM is calculated as 810–900 cycles with the TGO thickness between 6.4 and 6.6 μm , which agrees with experimental average lifetime 860 cycles.

Acknowledgments

We acknowledge the funding supports of the project (no. 50801005) from Chinese National Natural Science Foundation.

References

- [1] N.P. Padture, M. Gell, E.H. Jordan, Science 296 (2002) 280.
- [2] F. Traeger, M. Ahrens, R. Vaßen, D. Stover, Mater. Sci. Eng., A 358 (2003) 255.
- [3] M. Caliez, J.-L. Chaboche, F. Feyel, S. Kruch, Acta Mater. 51 (2003) 1133.
- [4] R.A. Miller, C.E. Lowell, Thin Solid Films 95 (1982) 265.
- [5] O. Trunova, T. Beck, R. Herzog, L. Singheiser, Surf. Coat. Technol. 202 (2008) 5027.
- [6] T. Beck, R. Herzog, O. Trunova, M. Offermann, R.W. Steinbrech, L. Singheiser, Surf. Coat. Technol. 202 (2008) 5901.
- [7] C.H. Hsueh, E.R. Fuller, Scr. Mater. 42 (2000) 781.
- [8] V. Robert, G. Stephan, D. Stover, J. Therm. Spray Technol. 18 (2009) 835.
- [9] R. Vaßen, G. Kerkhoff, D. Stover, Mater. Sci. Eng., A 303 (2001) 100.
- [10] E.P. Busso, Z.Q. Qian, M.P. Taylor, H.E. Evans, Acta Mater. 57 (2009) 2349.
- [11] E.P. Busso, J. Lin, S. Sakurai, M. Nakayama, Acta Mater. 49 (2001) 1515.
- [12] E.P. Busso, J. Lin, S. Sakurai, Acta Mater. 49 (2001) 1529.
- [13] J. Rosler, M. Baker, K. Aufzug, Acta Mater. 52 (2004) 4809.
- [14] J. Rosler, M. Baker, M. Volgmann, Acta Mater. 49 (2001) 3659.
- [15] M. Baker, J. Rosler, G. Heinze, Acta Mater. 53 (2005) 469.
- [16] E.P. Busso, L. Wright, H.E. Evans, L.N. McCartney, S.R.J. Saunders, S. Osgerby, J. Nunn, Acta Mater. 55 (2007) 1491.
- [17] E.P. Busso, H.E. Evans, L. Wright, L.N. McCartney, J. Nunn, S. Osgerby, Mater. Corros. 59 (2008) 556.
- [18] C. Zhou, N. Wang, Z. Wang, S. Gong, H. Xu, Scr. Mater. 51 (2004) 945.
- [19] O. Trunova, Effect of Thermal and Mechanical Loadings on the Degradation and Failure Modes of APS-TBCs, PhD thesis, Westfaelische Technische Hochschule, Aachen, Germany, 2006.
- [20] P. Bednarz, Finite Element Simulation of Stress Evolution in Thermal Barrier Coating Systems, Jülich, PhD thesis, Forschungszentrum Jülich GmbH, Germany, 2006.
- [21] H. Bhatnagar, Computational Modeling of Failure in Thermal Barrier Coatings under Cyclic Thermal Loads, PhD thesis, The Ohio State University, Ohio State, USA, 2009.
- [22] S. Wei, W. Fu-chi, F. Qun-bo, H. Dan, M. Zhuang, Surf. Coat. Technol. 205 (2011) 2964.